This is an open access article published under an ACS AuthorChoice License, which permits copying and redistribution of the article or any adaptations for non-commercial purposes.

ACS OMEGA

Article

Cite This: ACS Omega 2018, 3, 7962−7970

Antibacterial and Photocatalytic Properties of ZnO−9-Aminoacridine Hydrochloride Hydrate Drug Nanoconjugates

Piyali Mitra,[†] Debanjan Dutta,[‡] Somnath Das,[§] Tarakdas Basu,[‡] Amitava Pramanik,[§] and Amitava Patra*,[†]

[†]Department of Materials Science, Indian Association for the Cultivation of Science, Kolkata 700032, India

[‡]Department of Biochemistry and Biophysics, University of Kalyani, Kalyani 741235, West Bengal, India

[§]Unilever R&D Bangalore, 64, Main Road, Whitefield, Bangalore 560066, India

Supporting Information

ABSTRACT: The development of nanomaterial-based hybrid systems for healthcare and energy-related materials has attracted significant attention nowadays. Here, we have designed a nanocomposite of ZnO nanoparticles (NPs) with anticancer therapeutic drug 9-aminoacridine hydrochloride hydrate (9AA-HCl) for antibacterial and photocatalytic activities. Spectroscopic studies reveal that the photoinduced electron transfer from photoexcited 9AA-HCl to the conduction band of ZnO NP causes the generation of the reactive oxygen species (ROS), which is responsible for antibacterial activity and photocatalytic properties. It is seen that the efficiency of photodegradation of dye molecules increases in ZnO−9AA-HCl nanoconjugated systems than pure ZnO nanoparticles because of efficient charge separation. In addition, the antibacterial efficacy of the nanoconjugate is investigated using a strain of Gram-negative bacteria where the cell-killing activities are observed 99.99 and 100% for 20 and 21 μL/mL nanoconjugate, respectively, and very little cell-killing activity is observed for free ZnO NPs and free drug. Moreover, it is also observed that the nanoconjugate generates sufficient intracellular ROS that can hydrolyze 2′,7′-dichlorodihydrofluoresceindiacetate (DCFH-DA) to highly fluorescent 2′,7′-dichlorofluorescein (DCF). The outcome of the study will provide valuable information for designing new-edge nanoconjugate materials for potential applications in photocatalytic and antibacterial activities.

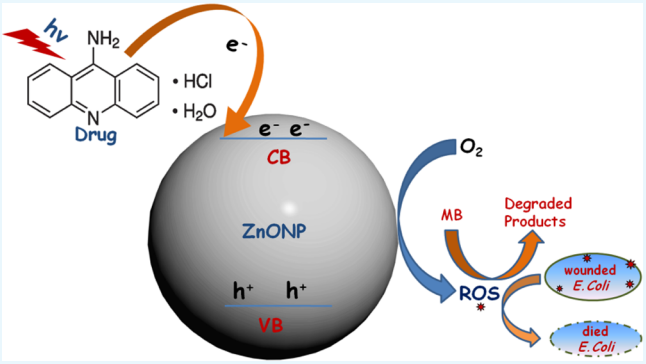

INTRODUCTION

Oxide nanomaterials are found to have potential for various applications such as light harvesting and healthcare. Among them, ZnO and TiO_2 are the most used oxide nanomaterials for hydrogen generation, sunscreen, antimicrobial activity, and photocatalysis.[1−5] Zinc oxide nanoparticles (ZnO NPs) have several advantages such as high photosensitivity, thermal stability, low toxicity, and good biocompatibility, which are important for photocatalytic and biological applications.[6−8] Yuan et al. have used ZnO quantum dots for tumor-targeted drug delivery[8] after combination with chitosan and doxorubicin (DOX). A pH-responsive drug delivery system has been designed by Liu et al. where the anticancer drug DOX is conjugated with ZnO NP.[9] It is also found that noble metal/zinc oxide hybrid materials are being used for water purification and different pathogenic applications.[10−14] ZnO nanostructured materials are generally insoluble in biological environment, whereas they can dissolve in an acidic biological environment.[6,15−17] However, the surface of ZnO NP is affected in a strong basic condition.[18] It is also seen that ZnO NPs are being used for nanocarriers for enhancing the release process.[19]

ZnO composite materials with polymers, bioimaging dye, and photodynamic therapeutic (PDT) drugs have been designed for bioapplications because of easy functionalization of the surface of ZnO NPs.[20−22] In PDT drugs, the photosensitive dye molecules are being excited by visible or near-infrared wavelength of light and subsequently the excited energy is transferred to the surroundings for the generation of highly reactive oxygen species (ROS) such as superoxide, hydroperoxyl, and hydroxyl radicals.[23−26] The multifunctional features of ZnO materials inspired us to develop a conjugate system (inorganic−organic hybrid) of ZnO NP with antibacterial therapeutic drug, 9-aminoacridine hydrochloride hydrate (9AA-HCl). Different pH-dependent forms of 9-aminoacridine hydrochloride hydrate (9AA-HCl) are given in Scheme 1.[27] Moreover, 9AA-HCl drug is a very important drug

Received: March 26, 2018
Accepted: July 5, 2018
Published: July 17, 2018

Downloaded via 65.21.193.86 on February 24, 2022 at 16:52:50 (UTC).
See https://pubs.acs.org/sharingguidelines for options on how to legitimately share published articles.

Scheme 1. Different Forms of 9-Aminoacridine Hydrochloride Hydrate (9AA-HCl)[a]

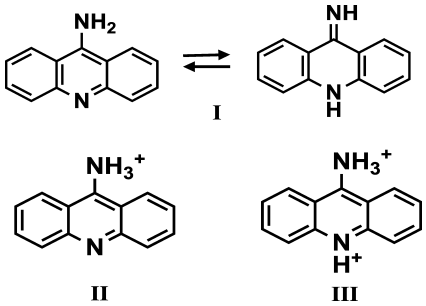

[a](I) Neutral 9AA-HCl (9AA), (II) protonated 9AA-HCl ($9AAH^+$), and (III) doubly protonated 9AA-HCl.

for antibacterial, mutagenic, and antitumor activities.[28−31] 9AA-HCl is being used as a DNA intercalation agent also.[28,29,32] Encapsulation of this drug inside the silica nanoparticles is also used for imaging the membranes.[33] It is reported that the antibacterial activity of 9AA-HCl is greatly enhanced after conjugation with gold nanoparticles.[34] Sardar et al. also reported the influence of protoporphyrin−ZnO nanohybrid on the growth of *Escherichia coli*.[35] It is found that the generation of ROS is the key factor for photochemical and photophysical processes between PDT drug and semiconductor nanoparticles. The photocatalytic activity of the inorganic semiconductor is controlled by ROS generation because ROS oxidize the organic compound.[36−39] The recombination of photogenerated electron and hole in semiconducting nanoparticles controls the photocatalytic efficiency, and the efficiency of photocatalysis is decreased because of the fast recombination process compared to the surface redox reactions.[40,41] Therefore, inorganic−organic hybrid nanomaterials are most useful for such applications because of the efficient charge transfer (electron or hole transfer) process and reduce the recombination of the electron−hole pairs.[41−46] Here, ZnO NP−9AA-HCl nanocomposite has been designed to investigate the influence of charge separation on photocatalytic and antibacterial activity. Steady-state and time-resolved spectroscopic studies are being used to investigate the charge transfer process in ZnO NP−9AA-HCl nanocomposite. Analysis reveals that the electron transfer from the drug molecule to the semiconductor occurs after photoexcitation, which consequently influences the photocatalytic efficiency as well as the antibacterial efficacy of the hybrid system. A strain of Gram-negative bacteria is being used for the antibacterial efficacy of drug-coated ZnO NPs.

■ RESULTS AND DISCUSSION

We have synthesized ZnO NP in a solution phase technique using the earlier work.[47,48] The transmission electron microscopy (TEM) micrograph of synthesized ZnO NP is presented in Figure S1A. The monodisperse ZnO NPs of size ~6.2 ± 0.5 nm are synthesized using TMOH (Figure S1B). Figure 1 illustrates the TEM image of 9AA-HCl−ZnO nanohybrid, which confirms the consistency of nearly spherical nanocrystals.

The binding nature between the 9AA-HCl drug and ZnO NP is investigated using Fourier-transform infrared (FTIR) technique as the attachment is very crucial for biological applications. The FTIR spectra of bare ZnO NP, 9AA-HCl, and nanoconjugate are presented in Figure 2. The characteristic peak of pure 9AA-HCl at 3337 cm^{-1} is due to the stretching frequency of the amine group ($-NH_2$).[34] After conjugation with ZnO NP, the stretching frequency of the amine moiety of the drug is shifted and broadened. The shifting of the stretching frequency clearly indicates the covalent bonding formed between the amine group and ZnO NP.[35,49] The broad band around 3370−3400 cm^{-1} and sharp band around 1630−1635 cm^{-1} are due to surface hydroxyl groups of ZnO,[50,51] which are affected after conjugation with the drug molecule. The shifting of band position of −OH stretching suggests the formation of hydrogen bonding between ZnO NP and 9AA-HCl.[52,53]

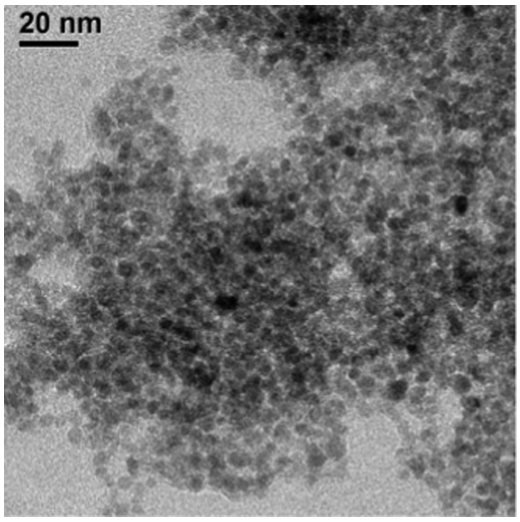

Figure 1. Transmission electron micrograph of the nanoconjugate (ZnO−9AA-HCl).

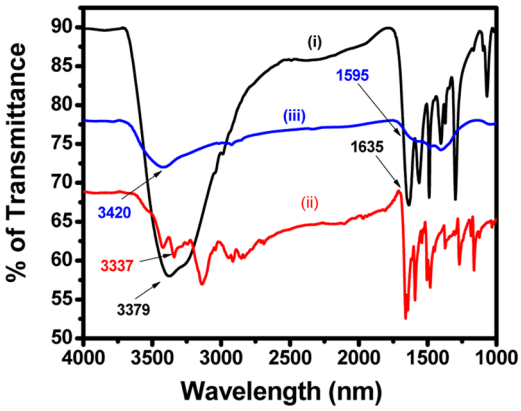

Figure 2. FTIR spectra of bare ZnO (i), only 9AA-HCl (ii), and ZnO−9AA-HCl conjugate (iii).

Raman spectra of ZnO NP and after conjugation with 9AA-HCl are shown in Figure 3. No Raman band is observed in 9AA-HCl in the wavenumber range from 300 to 600 cm^{-1} because of its highly fluorescent molecule after excitation at 532 nm. According to space group theory, the Raman active vibrational modes of ZnO structure are $A_1 + 2E_2 + E_1$. As evident from the figure, four vibration peaks at 328, 378, 438, and 577 cm^{-1} of ZnO NP confirm the presence of a wurtzite structure.[51,54] The strong band at 438 cm^{-1} is a nonpolar

DOI: 10.1021/acsomega.8b00568
ACS Omega 2018, 3, 7962−7970

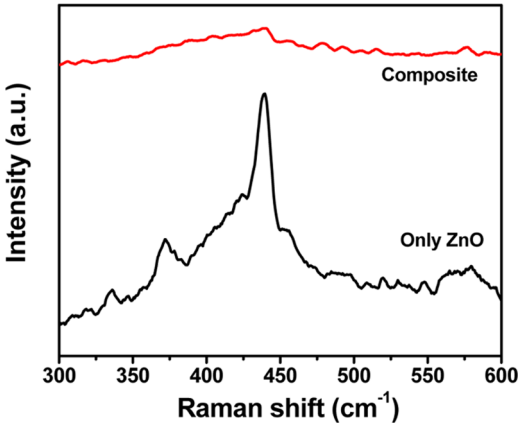

Figure 3. Raman spectra of ZnO NP (black) and 9AA-HCl−ZnO NPs (red).

optical phonon E_2 mode of ZnO NP, which is due to the oxygen deficiency. The peaks at 378 and 577 cm^{-1} are due to the polar transverse A_1 and longitudinal E_1 optical phonon mode, respectively. The peak at 332 cm^{-1} is assigned to the $E_2^{high}-E_2^{low}$ mode.[51] It is noted that the E_2 mode (due to defect centers) of ZnO NP is significantly changed after conjugation of 9AA-HCl with ZnO NP, indicating the passivation of the ZnO NPs surface with 9AA-HCl.

Steady-State and Time-Resolved Spectroscopic Studies of a ZnO−9AA-HCl System. The formation of ZnO−9AA-HCl nanohybrid is characterized by UV−vis spectroscopy. The photodynamic therapeutic drug, 9AA-HCl, has two pK_a values of −2.0 and 10.0.[55] At pH < −2.0, that is, in the presence of concentrated strong acid, the doubly protonated form predominates, whereas within −2.0 < pH < 10.0, the protonated form, that is, $9AAH^+$ prevails. In pH > 10.0, the neutral 9AA-HCl, that is, 9AA is formed through the deprotonation of $9AAH^+$ and it retains equilibrium between its amino and imino tautomers.[56] Figure S2A,B illustrates that the absorption peaks and the fluorescence peaks of the neutral form of 9AA-HCl, that is, 9AA at pH = 11.0 are slightly red shifted compared to that of the protonated form of 9AA-HCl, that is, $9AAH^+$ at pH = 4.0. Figure 4 displays the absorption spectra of bare ZnO NP, 9AA-HCl, and ZnO−9AA-HCl composite. The ZnO NPs exhibit a threshold (i.e., band gap) at 345 nm (3.59 eV), and 9AA-HCl has maximum absorbance at 400 nm. No distinct peak of 9AA-HCl is observed in the absorption spectrum of nanoconjugate because of the very low concentration of drug molecule and the large scattering of the ZnO NPs. The UV absorption peak of the nanoconjugate is slightly blue shifted compared to ZnO, with an onset at 338 nm (3.67 eV). Analysis reveals that ZnO−9AA-HCl nanoconjugate is formed by the interaction between ZnO and the amine group of 9AA-HCl and not by the physical absorption.

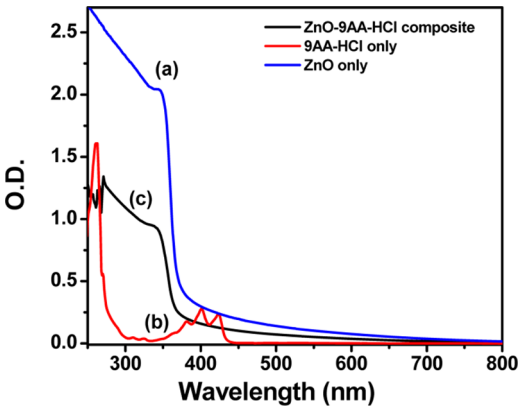

Figure 4. UV−vis absorption spectra of (a) ZnO NP, (b) 9AA-HCl, and (c) ZnO−9AA-HCl.

Recently, it has been demonstrated that the photocurrent generation is due to efficient charge separation between ZnO NP and carbon dot.[47] Again, laser flash photolysis study reveals the photoinduced electron transfer (PET) between ZnO NP and methyl viologen.[48] It is reported that the visible (green) emission from ZnO NPs arises due to oxygen vacancies.[57] We monitored ZnO emission in the absence and the presence of 9AA-HCl (Figure 5A), and it is noteworthy that the visible emission of ZnO NP is caused by the surface states because the surface of the particle is modified by the presence of the drug molecules. Herein, the possibility of energy transfer is ruled out because there is no spectral overlap between them. Thus, the emission quenching in the visible region is solely due to photoinduced electron transfer. Here, we have also observed that the emission of 9AA-HCl is quenched and blue shifted after attachment with ZnO NP (Figure 5B). It is to be mentioned that the photoluminescence (PL) spectrum of 9AA-HCl is almost identical with its neutral from (as mentioned in Figure S2B) after conjugation with ZnO NP. This result suggests that the neutral form of 9AA-HCl predominates and forms hydrogen bonding with ZnO NP, which is well supported by FTIR studies as mentioned in the earlier section.

To understand the charge transfer between ZnO NP and 9AA-HCl, all of the samples were analyzed by time-resolved fluorescence spectroscopy. The measurements were carried out by exciting 9AA-HCl at 371 nm and monitoring emission at 455 nm. Figure 6 displays the emission decay profile of only 9AA-HCl and the nanoconjugate. These emission decay times are analyzed using exponential decay kinetics, and the parameters of samples (9AA-HCl and nanoconjugate) are summarized in Table S1. The average decay time is measured using the decay components.[58] The almost similar decay times of the neutral and singly protonated species were obtained, which are consistent with the earlier work.[59] Figure 6 shows the fluorescence decay curve of 9AA-HCl, which is fitted with single-exponential decay, and the lifetime is 12.89 ns. In comparison, for ZnO−9AA-HCl nanohybrid, the fluorescence decay profile is composed of a faster component of 0.65 ns (78%) and a slower component of 12.87 ns (22%). Although the slower component is consistent with the excited-state lifetime of 9AA-HCl without ZnO, the faster one may be due to the electron transfer from 9AA-HCl to ZnO NP.[60] The decay time decreases from 12.89 to 3.34 ns, suggesting the photoinduced electron transfer (PET) from the lowest unoccupied molecular orbital of 9AA-HCl to the conduction band of semiconductor via nonradiative pathway.[60] The nonradiative rate constant (k_{nr}) is determined by comparing the decay time of 9AA-HCl in the absence (τ_o) and in the presence (τ) of ZnO NP, using the following equation

$$k_{nr} = \frac{1}{\langle\tau\rangle} - \frac{1}{\langle\tau_0\rangle} \quad (1)$$

The rate of the electron transfer process from the excited state of 9AA-HCl to the conduction band of ZnO NP is estimated to be 1.54×10^9 s^{-1} (considering only the faster component), which is consistent with the value reported in the literature.[60]

DOI: 10.1021/acsomega.8b00568
ACS Omega 2018, 3, 7962−7970

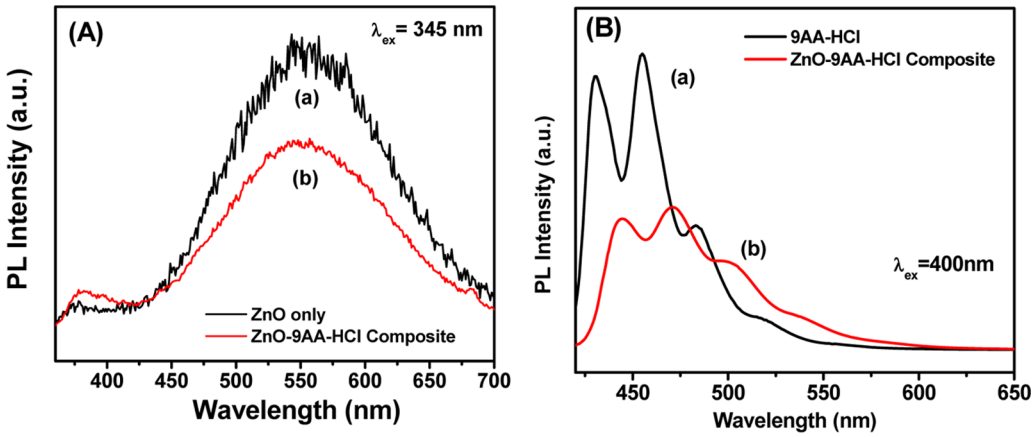

Figure 5. (A) Room-temperature PL spectra (excitation wavelength was at 345 nm) of (a) bare ZnO and (b) ZnO-anchored 9AA-HCl. (B) Room-temperature PL spectra (excitation wavelength was at 400 nm) of (a) bare 9AA-HCl and (b) ZnO-anchored 9AA-HCl.

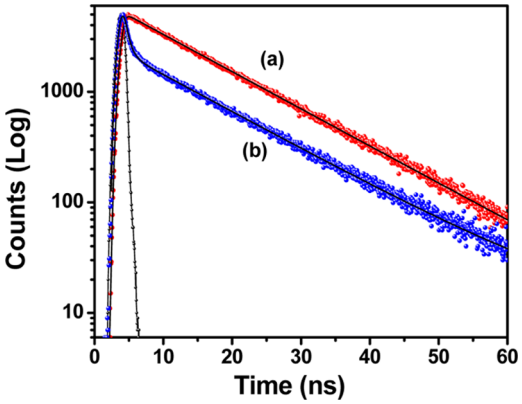

Figure 6. Time-resolved decay curves of (a) 9AA-HCl and (b) the conjugate (ZnO NP−9AA-HCl): (Ex 371 nm and Em 455 nm).

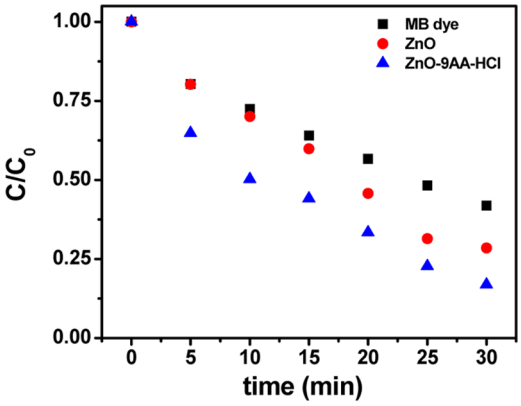

Figure 7. Photocatalytic degradation of MB in the presence of ZnO (red) and ZnO−9AA-HCl (blue).

Therefore, the interfacial PET from the excited state of 9AA-HCl to ZnO NP reduces the recombination of electron and hole of semiconductor, which enhances the photocatalytic activity as well as the biological activity which will be discussed in the further course of discussion.

Photocatalytic Activity Study. The charge transportation and separation are considered to be key factors for improving the photocatalytic activity.[42] Here, we have studied the degradation pattern of methylene blue (MB) dye in the presence of ZnO−9AA-HCl composite to establish the photocatalytic efficacy. It is well established that MB undergoes degradation in the presence of UV light and this can be enhanced by photocatalysts such as ZnO. It is seen from Figure 7 that the photodegradation efficiency after 30 min of irradiation increases in the presence of 9AA-HCl and the efficiencies are 72 ± 0.45 and 83.6 ± 0.22% for ZnO NP and the ZnO−9AA-HCl conjugate, respectively. Moreover, it is evident from the obtained results that the kinetics of dye degradation follows pseudo-first-order and the rate of degradation is in the order MB < ZnO NPs < composite. The calculated rate constants for the samples MB, ZnO NP, and composite are found to be 0.013, 0.018, and 0.026 min^{-1} respectively. The enhanced photocatalytic activity (conjugate has ∼1.44 times higher catalytic activity than that of the only ZnO NP) is explained by the enhanced charge separation in the composites, compared to bare ZnO NPs. During photocatalytic reaction, the photoexcited 9AA-HCl transfers an electron to the conduction band of ZnO NPs which consequently generates reactive oxygen species (ROS) in the presence of oxygen and water that can degrade the organic pollutant. The proposed mechanism of ROS generation is described below. The valence band holes can oxidize a large number of organic pollutants into CO_2 and H_2O, whereas conduction band electrons are strong reducing agents which will be adsorbed by O_2 to form a superoxide anion which is strongly oxidizing and further oxidizes organic pollutants into CO_2 and H_2O. Therefore, analysis suggests that ZnO−9AA-HCl composite is an efficient photocatalytic material that enhances the decomposition of aqueous organic pollutant MB.

Mechanism.

$$\text{Drug (9AA-HCl)} + h\nu \rightarrow \text{drug} \times (e^- \cdots h^+)$$

$$\text{Drug} \times (e^- \cdots h^+) + \text{ZnO NP} \rightarrow \text{ZnO NP } (e^-_{CB}) + \text{drug } (h^+)$$

$$\text{ZnO NP } (e^-_{CB}) + O_2 \rightarrow O_2^{\bullet -} + \text{ZnONP}$$

$$O_2^{\bullet -} + H_2O \rightarrow HO_2^{\bullet} + OH^-$$

$$HO_2^{\bullet} + H_2O \rightarrow OH^{\bullet} + H_2O_2$$

$$H_2O_2 \rightarrow 2OH^{\bullet}$$

$$\text{Drug } (h^+) + H_2O \rightarrow OH^{\bullet} + H^+$$

DOI: 10.1021/acsomega.8b00568
ACS Omega 2018, 3, 7962−7970

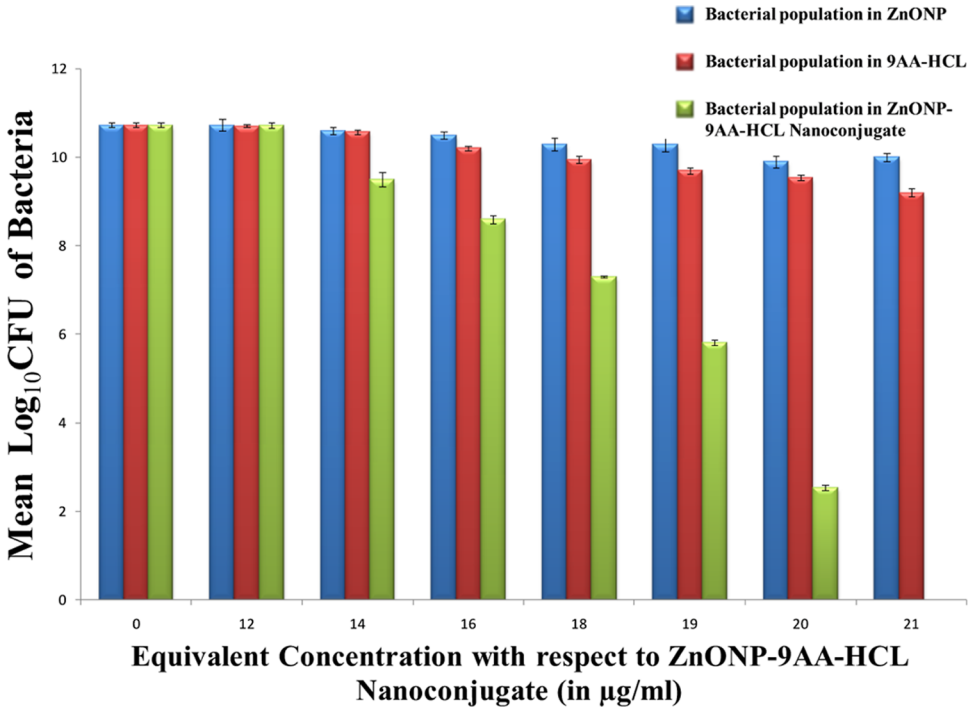

Figure 8. Antibacterial activity study where green bars represent nanoconjugate-exposed cells, blue and red bars represent only ZnO NP, free drug 9AA-HCl (of equivalent concentrations as present in the nanoconjugate) exposed cells, respectively. Data are the mean of three replications with ±standard error.

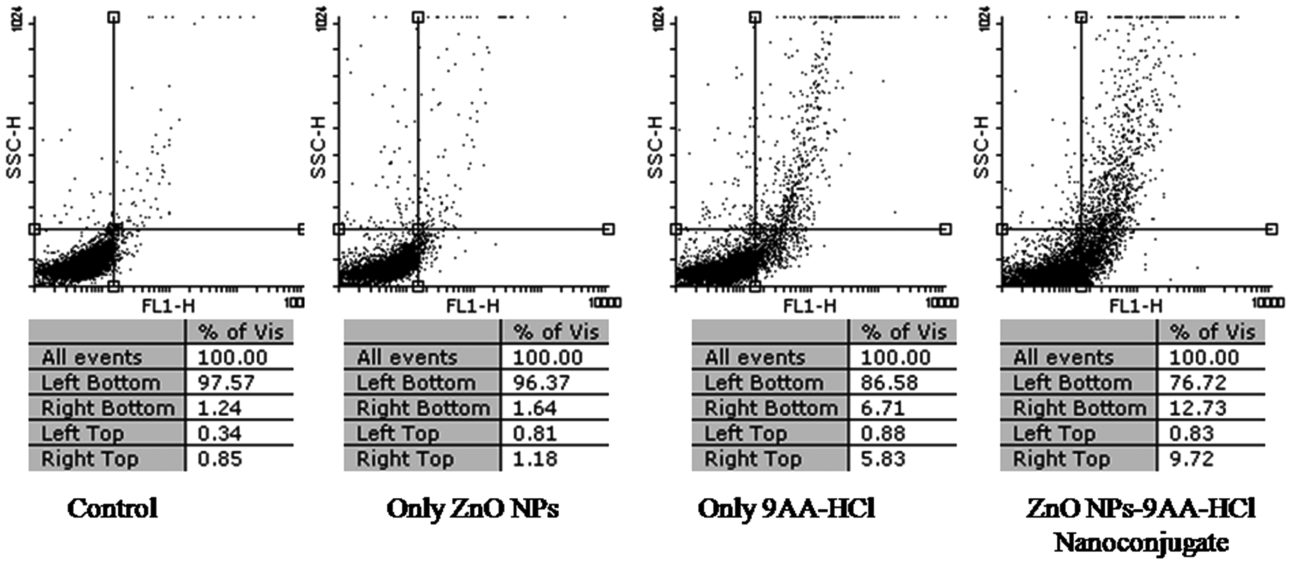

Figure 9. Flow cytometric analysis of intracellular ROS generation study of control, only ZnO NP, free drug, and the nanoconjugate-exposed cells at their MIC value for 1 h.

$$OH^{\bullet} + MB \rightarrow \text{products (degraded MB} + CO_2 + H_2O + NH_4^+ + NO_3^- + SO_4^{2-} + Cl^-)$$

Antibacterial Activity of the Nanoconjugate. For antibacterial activity of this nanocomposite, the study was conducted on the *E. coli* K12 bacteria to determine the antibacterial potency of only ZnO NP, only 9AA-HCl, and the nanoconjugate. The bacterial cells were exposed to different concentrations of the respective sample in medium for 18 h and followed by their viability determination from colony counts on agar plates. The result depicted that the bacterial cell numbers are static, that is, 2×10^5 up to the concentration of 18 μL/mL of nanoconjugate after 18 h incubation because bacterial population did not increase and is nearly the same with that of the initial population. Thus, this concentration is considered the minimum inhibitory concentration (MIC) of the nanoconjugate for *E. coli* K12. Above this concentration of the nanoconjugate, the cell-killing takes place. The cells killing is 99.99 and 100% for the concentrations of 20 and 21 μL/mL, respectively. Therefore, the minimum bactericidal concentration (MBC) of the nanoconjugate is between 20 and 21 μL/mL. However, results of control experiments showed that free

DOI: 10.1021/acsomega.8b00568
ACS Omega 2018, 3, 7962−7970

ZnO NPs have no such kind of superior bactericidal activity and the free drug has very little cell-killing activity (Figure 8).

Figure 9 depicts the percentage distributions of cells in different quadrants. Increase in intracellular ROS will result in a shift of the cell populations to the higher fluorescent quadrant, that is, toward right side quadrant. The cells were treated at their minimum inhibitory concentration (MIC) values to check whether this concentration of nanocomposite is able to generate sufficient intracellular ROS that can hydrolyze 2′,7′-dichlorodihydrofluoresceindiacetate (DCFH-DA) to highly fluorescent 2′,7′-dichlorofluorescein (DCF). For control-labeled cells, nearly 98% of cells are present in the left lower quadrant (Figure 9). The treatment of bacterial cells with only ZnO NPs and only 9AA-HCl does not elicit the intracellular ROS that much. However, when the cells were treated with the ZnO NPs−9AA-HCl nanoconjugate at their MIC value for 1 h, about 23% of cells acquired a considerable higher fluorescence, that is, high level of ROS. Therefore, analysis reveals that the nanoconjugate kills bacteria through ROS-mediated pathways.

It is reported that the toxicity mechanism of ZnO NPs varies in various media as the species of dissolved Zn may change.[61] ROS generation is also known as the major cause of nanotoxicity.[62−65] The toxicity of these species involves the destruction of cellular components such as lipids, DNA, and proteins as a result of their internalization into the bacterial cell membrane. Here, the results clearly indicate that the enhanced ROS generation in the presence of the nanoconjugate increases the antibacterial activity compared to the free drug and free ZnO NP. The reason behind the enhanced activity implies that the presence of ZnO NP in the proximity of 9AA-HCl facilitates the charge separation along with the increase of Zn^{2+} ions. Once nanoconjugates are in the growth media, they will carry on releasing peroxides covering the entire surfaces of the dead bacteria. Therefore, this continuous peroxide (because the increase of H^+ in the medium enhances the amount of H_2O_2) release leads to higher bactericidal efficacy.

■ CONCLUSIONS

Here, the semiconductor-therapeutic drug nanoconjugate exhibits enhancement in photocatalytic activity and antibacterial activity toward Gram-negative bacteria because of the generation of charge carriers and ROS. The considerable changes in photophysical properties of 9AA-HCl are observed after conjugation with ZnO NPs. The steady-state and time-resolved fluorescence studies signify the fact that photoinduced electron transfer (PET) occurs from 9AA-HCl to the conduction band of ZnO NP. Moreover, the shifting of PL emission of 9AA-HCl, which resembles the neutral form of 9AA-HCl, indicates the fact that the H-bonding occurs between 9AA-HCl and ZnO NPs. Utilizing the charge transfer phenomena, we have studied the photocatalytic property of the nanoconjugate, which shows that the kinetics of MB dye degradation follows pseudo-first-order and the rate of degradation is in the order MB < ZnO NPs < nanoconjugate. In addition, the nanoconjugate possesses superior antibacterial activity against *E. coli* K12 compared to the free ZnO NPs and free drug. The enhanced ROS generation in the reaction medium for the nanoconjugate is the main reason behind such activity. Our investigation on the photoinduced dynamics of ZnO NPs upon complexation with the anticancer drug 9AA-HCl may open the avenue to utilize the unique electron-accepting property of the semiconductor in the development of the photocatalyst as well as drug delivery vehicles.

■ EXPERIMENTAL SECTION

Materials and Methods. *Materials.* 9-Aminoacridine hydrochloride hydrate (9AA-HCl) and zinc acetate dihydrate (Sigma-Aldrich) were used. Tetramethyl ammonium hydroxide (Merck) (TMOH), spectroscopic-grade ethanol, methanol and HPLC water (Merck) were used for the synthesis and experiment in the present study.

Synthesis of ZnO Nanoparticles. We prepared ZnO nanoparticles (ZnO NPs) using the previously reported method.[66] Zinc acetate dihydrate (0.22 g) was dissolved in 80 mL of ethanol. The temperature of the solution was raised to 100 °C after complete dissolution of zinc acetate. Then, 3 mL solution of tetramethyl ammonium hydroxide (TMOH, 0.86 g in methanol) was added slowly to the ethanolic solution of zinc acetate under stirring at 100 °C. The solution was then allowed to boil for another 30 min. The solution color turned from colorless to white, and it was cooled down under stirring condition. ZnO NP was precipitated by centrifugation at 10 000 rpm for 10 min and further dissolved in ethanol and centrifuged. Washing was carried out several times to remove the excess precursor. The obtained ZnO NPs are used for the further study.

Synthesis of 9-Aminoacridine Hydrochloride Hydrate−Zinc Oxide Nanoparticle (9AA-HCl−ZnO NP) Nanoconjugates (Sensitization of 9AA-HCl on the Surface of ZnO NPs). An ethanolic solution of 0.5 mL of 9AA-HCl was prepared under stirring. Then, this ethanolic solution of 9AA-HCl was added with ZnO NPs under stirring condition for 6 h. After the sensitization process, the obtained solution was centrifuged for a few minutes and the clear supernatant solution containing the unattached drug was removed. After that, washing was carried out several times to remove any unattached drug. The nanoconjugate was then dried and stored for further use. For all characterizations, we dissolve the nanoconjugate in ethanol.

Characterization. A transmission electron microscope (TEM) having model JEOL-TEM-2100F was used for the morphological study of as synthesized nanoparticles. A UV−vis spectrophotometer (Shimadzu) and a Fluoro Max-P (HORIBA JOBIN YVON) photoluminescence spectrophotometer were used for the optical study. A Horiba Jobin Yvon Raman spectrometer using a helium−neon laser at an excitation wavelength of 532 nm was used. A Shimadzu (FTIR-8300) spectrometer was used for Fourier-transform infrared (FTIR) spectroscopy measurements, using KBr pellets. In time-correlated single-photon counting measurement, the samples were excited at 375 nm using a picosecond diode laser (NANO-LED IBH 370L) and the fluorescence decays were analyzed using IBH DAS6 software. To analyze the fluorescence decays, the following equation was used, $P(t)$[67]

$$P(t) = b + \sum_{i}^{n} \alpha_i \exp\left(-\frac{t}{\tau_i}\right) \tag{2}$$

here, n is the number of discrete emissive species and b is the baseline correction ("dc" offset). The pre-exponential factors and excited-state fluorescence lifetimes associated with the i component are α_i and τ_i, respectively. The average lifetime $\langle\tau\rangle$ for multiexponential decays was estimated using the following equation

DOI: 10.1021/acsomega.8b00568
ACS Omega 2018, 3, 7962−7970

$$\langle \tau \rangle = \sum_{i=1}^{n} \beta_i \tau_i \quad (3)$$

where $\beta_i = \alpha_i / \sum \alpha_i$ and β_i is the contribution of the decay component.

Photocatalytic Activity. The photocatalytic activity of ZnO and its composite with 9AA-HCl were monitored using methylene blue dye (MB) solution. In 100 mL of 20 μM methylene blue solution, 5 mg of particle was added, allowed to stand in dark for 30 min, and then transferred to a photocatalytic reactor. UV light from a mercury lamp (60 W, 365 nm) was used to irradiate the particle suspension under constant stirring condition (at 250 rpm, 25 °C). Finite amounts of aliquot were withdrawn at an interval of 5 min, and absorbance was recorded at 664 nm using a UV−vis spectrophotometer. The degradation pattern of blank dye in the absence of the catalyst was also performed under identical condition.

Biological Activity Study. *Analysis of Antibacterial Activity of ZnO NPs.* The antibacterial properties of the samples were determined by selecting the Gram-negative bacterium *E. coli* K12. All of the experiments were done with freshly grown overnight culture of *E. coli* cells.

Determination of the Minimum Inhibitory Concentration (MIC) and Minimum Bactericidal Concentration (MBC) of ZnO NPs. The MIC of an antibacterial agent for a specific bacterium is defined as the concentration of the antibacterial agent in the growth medium that causes the complete inhibition of bacterial growth without killing the bacteria even after overnight incubation. MBC is the concentration of an antimicrobial substance needed for killing 99.9% of the bacterial population.[50] The MIC and MBC values were determined by counting the number of bacterial colonies found on a nutrient-agar plate after 24 h of incubation at 37 °C. The detailed procedure is as follows: the overnight grown culture of *E. coli* K12 was inoculated into fresh nutrient broth (Himedia Laboratories, India) at a final concentration of 5×10^7 cells/mL. This fresh culture was divided into different parts (to 5 mL each) to treat with different concentrations of ZnO NPs. All of the treated 5 mL of cultures were incubated at 37 °C with shaking for 18 h. Cell aliquot of 100 μL was withdrawn from each of the individual cultures, diluted, and spread over nutrient-agar plates to assay the number of viable cells.[68]

Measurement of Intracellular ROS Production. The comparative ROS production in ZnO NPs, 9AA-HCl, and the nanoconjugate-exposed bacterial cells was estimated using the dye 2′,7′-dichlorodihydrofluoresceindiacetate (DCFH-DA). To determine the intracellular ROS, approximately 10^7 order of cells were treated with only ZnO NPs, only 9AA-HCl, and ZnO NP−9AA-HCl nanoconjugate at the MIC value for 1 h (equivalent amount with respect to ZnO NP−9AA-HCl nanoconjugate) and then subsequently washed twice with phosphate-buffered saline (PBS). DCFH-DA (10 μM) was then added to the cells and the cells were incubated in the dark for 30 min at 37 °C. Cells were washed twice with PBS and analyzed by a flow cytometer (FACS Calibur; Becton Dickinson) through the FL1-H channel. The data were plotted as histogram using Flowing Software 2.5.1 (University of Turku). After diffusion into the cells, the dye was deacetylated by cellular esterases to a nonfluorescent compound, which was later oxidized by ROS into 2′,7′-dichlorofluorescein (DCF).[69,70] This is a highly authentic method for the determination of intracellular reactive oxygen species (ROS).

■ ASSOCIATED CONTENT

Supporting Information

The Supporting Information is available free of charge on the ACS Publications website at DOI: 10.1021/acsomega.8b00568.

Transmission electron micrographs of only ZnO NP; particle size distribution diagram of ZnO NP; the absorption spectra of 9AA-HCl (6×10^{-5} M) in water at different pH values; fluorescence spectra of 9AA-HCl (6×10^{-5} M) in water at different pH values (λ_{ex} = 400 nm); time-resolved decay parameters of only drug and the composite, measured at 455 nm under 371 nm excitation wavelength (PDF)

■ AUTHOR INFORMATION

Corresponding Author

*E-mail: msap@iacs.res.in. Tel: (91)-33-2473-4971. Fax: (91)-33-2473-2805.

ORCID

Amitava Patra: 0000-0002-8996-9015

Notes

The authors declare no competing financial interest.

■ ACKNOWLEDGMENTS

P.M. thanks DST for awarding fellowship and financial support (the Fellowship reference no. PDF/2016/000509). P.M. also thanks IACS for the support throughout experiments. Unilever Industries Private Ltd. is gratefully acknowledged. We thank Monoj Kumar Barman, Rajesh Bera, and Bikash Jana for their valuable input.

■ REFERENCES

(1) Kundu, S.; Patra, A. Nanoscale Strategies for Light Harvesting. *Chem. Rev.* **2017**, *117*, 712−757.

(2) Leung, Y. H.; Chan, C. M. N.; Ng, A. M. C.; Chan, H. T.; Chiang, M. W. L.; Djurisic, A. B.; Ng, Y. H.; Jim, W. Y.; Guo, M. Y.; et al. Antibacterial Activity of ZnO Nanoparticles with a Modified Surface under Ambient Illumination. *Nanotechnology* **2012**, *23*, No. 475703 (1-12).

(3) Chen, X.; Mao, S. S. Titanium Dioxide Nanomaterials: Synthesis, Properties, Modifications, and Applications. *Chem. Rev.* **2007**, *107*, 2891−2959.

(4) Kubacka, A.; Fernandez-García, M.; Colon, G. Advanced Nanoarchitectures for Solar Photocatalytic Applications. *Chem. Rev.* **2012**, *112*, 1555−1614.

(5) Chen, C.; Ma, W.; Zhao, J. Semiconductor-Mediated Photodegradation of Pollutants under Visible-Light Irradiation. *Chem. Soc. Rev.* **2010**, *39*, 4206−4219.

(6) Xiong, H.-M. ZnO Nanoparticles Applied to Bioimaging and Drug Delivery. *Adv. Mater.* **2013**, *25*, 5329−5335.

(7) Barick, K. C.; Nigam, S.; Bahadur, D. Nanoscale Assembly of Mesoporous ZnO: A Potential Drug Carrier. *J. Mater. Chem.* **2010**, *20*, 6446−6452.

(8) Yuan, Q.; Hein, S.; Misra, R. D. K. New generation of Chitosan-Encapsulated ZnO Quantum Dots Loaded with Drug: Synthesis, Characterization and in vitro Drug Delivery Response. *Acta Biomater.* **2010**, *6*, 2732−2739.

(9) Liu, J.; Ma, X.; Jin, S.; Xue, X.; Zhang, C.; Wei, T.; Guo, W.; Liang, X.-J. Zinc Oxide Nanoparticles as Adjuvant to Facilitate Doxorubicin Intracellular Accumulation and Visualize pH-Responsive

DOI: 10.1021/acsomega.8b00568
ACS Omega 2018, 3, 7962−7970

Release for Overcoming Drug Resistance. *Mol. Pharmaceutics* **2016**, *13*, 1723−1730.
(10) He, W.; Kim, H.-K.; Wamer, W. G.; Melka, D.; Callahan, J. H.; Yin, J.-J. Photogenerated Charge Carriers and Reactive Oxygen Species in ZnO/Au Hybrid Nanostructures with Enhanced Photocatalytic and Antibacterial Activity. *J. Am. Chem. Soc.* **2014**, *136*, 750−757.
(11) Hu, J.; Zhong, Z.; Zhang, F.; Xing, W.; Jin, W.; Xu, N. High-efficiency, Synergistic ZnO-Coated SiC Photocatalytic Filter with Antibacterial Properties. *Ind. Eng. Chem. Res.* **2016**, *55*, 6661−6670.
(12) Kumar, R.; Anandan, S.; Hembram, K.; Rao, T. N. Efficient ZnO-Based Visible-Light-Driven Photocatalyst for Antibacterial Applications. *ACS Appl. Mater. Interfaces* **2014**, *6*, 13138−13148.
(13) Mao, C.; Xiang, Y.; Liu, X.; Cui, Z.; Yang, X.; Yeung, K. W. K.; Pan, H.; Wang, X.; Chu, P. K.; Wu, S. Photo-Inspired Antibacterial Activity and Wound Healing Acceleration by Hydrogel Embedded with Ag/Ag@AgCl/ZnO Nanostructures. *ACS Nano* **2017**, *11*, 9010−9021.
(14) Wang, Y.-W.; Cao, A.; Jiang, Y.; Zhang, X.; Liu, J.-H.; Liu, Y.; Wang, H. Superior Antibacterial Activity of Zinc Oxide/Graphene Oxide Composites Originating from High Zinc Concentration Localized around Bacteria. *ACS Appl. Mater. Interfaces* **2014**, *6*, 2791−2798.
(15) Cho, N.-H.; Cheong, T.-C.; Min, J. H.; Wu, J. H.; Lee, S. J.; Kim, D.; Yang, J.-S.; Kim, S.; Kim, Y. K.; Seong, S.-Y. A Multifunctional Core-Shell Nanoparticle for Dendritic Cell-Based Cancer Immunotherapy. *Nat. Nanotechnol.* **2011**, *6*, 675−682.
(16) Muhammad, F.; Guo, M.; Qi, W.; Sun, F.; Wang, A.; Guo, Y.; Zhu, G. pH-Triggered Controlled Drug Release from Mesoporous Silica Nanoparticles via Intracelluar Dissolution of ZnO Nanolids. *J. Am. Chem. Soc.* **2011**, *133*, 8778−8781.
(17) Abdelmonem, A. M.; Pelaz, B.; Kantner, K.; Bigall, N. C.; del Pino, P.; Parak, W. J. Charge and Agglomeration Dependent in vitro Uptake and Cytotoxicity of Zinc Oxide Nanoparticles. *J. Inorg. Biochem.* **2015**, *153*, 334−338.
(18) Zhou, J.; Xu, N. S.; Wang, Z. L. Dissolving Behavior and Stability of ZnO Wires in Biofluids: A Study on Biodegradability and Biocompatibility of ZnO Nanostructures. *Adv. Mater.* **2006**, *18*, 2432−2435.
(19) Zhang, Z. Y.; Xu, Y. D.; Ma, Y. Y.; Qiu, L. L.; Wang, Y.; Kong, J. L.; Xiong, H. M. Biodegradable ZnO@ Polymer Core-Shell Nanocarriers: pH-Triggered Release of Doxorubicin In Vitro. *Angew. Chem., Int. Ed.* **2013**, *52*, 4127−4131.
(20) Zhang, Y.; Nayak, T. R.; Hong, H.; Cai, W. Biomedical Applications of Zinc Oxide Nanomaterials. *Curr. Mol. Med.* **2013**, *13*, 1633−1645.
(21) Liu, D.; Wu, W.; Qiu, Y.; Yang, S.; Xiao, S.; Wang, Q.-Q.; Ding, L.; Wang, J. Surface Functionalization of ZnO Nanotetrapods with Photoactive and Electroactive Organic Monolayers. *Langmuir* **2008**, *24*, 5052−5059.
(22) Taratula, O.; Galoppini, E.; Wang, D.; Chu, D.; Zhang, Z.; Chen, H.; Saraf, G.; Lu, Y. Binding Studies of Molecular Linkers to ZnO and MgZnO Nanotip Films. *J. Phys. Chem. B* **2006**, *110*, 6506−6515.
(23) Dolmans, D. E.; Fukumura, D.; Jain, R. K. Photodynamic Therapy for Cancer. *Nat. Rev. Cancer* **2003**, *3*, 380−387.
(24) Girotti, A. W. Photosensitized Oxidation of Membrane Lipids: Reaction Pathways, Cytotoxic Effects, and Cytoprotective Mechanisms. *J. Photochem. Photobiol., B* **2001**, *63*, 103−113.
(25) Xue, L. Y.; Chiu, S. M.; Oleinick, N. L. Photochemical Destruction of the Bcl-2 Oncoprotein During Photodynamic Therapy with the Phthalocyanine Photosensitizer Pc 4. *Oncogene* **2001**, *20*, 3420−3427.
(26) Hong, I. S.; Greenberg, M. M. DNA Interstrand Cross-Link Formation Initiated by Reaction between Singlet Oxygen and a Modified Nucleotide. *J. Am. Chem. Soc.* **2005**, *127*, 10510−10511.
(27) Mitra, P.; Chakraborty, B.; Basu, S. A Spectroscopic Investigation of the Photophysical Behaviour of 9-Aminoacridine Hydrochloride Hydrate in Presence of Organic Amines in Homogeneous and Heterogeneous Media. *J. Lumin.* **2014**, *149*, 221−230.
(28) Zhu, H.; Clark, S. M.; Benson, S. C.; Rye, H. S.; Glazer, A. N.; Mathies, R. A High-Sensitivity Capillary Electrophoresis of Double-Stranded DNA Fragments Using Monomeric and Dimeric Fluorescent Intercalating Dyes. *Anal. Chem.* **1994**, *66*, 1941−1948.
(29) Rehn, C.; Pindur, U. Molecular Modeling of Intercalation Complexes of Antitumor Active 9-Aminoacridine and a [d,e]-Anellated Isoquinoline Derivative with base Paired Deoxytetranucleotides. *Monatsh. Chem.* **1996**, *127*, 645−658.
(30) Wynn, J. E.; Zhang, W.; Falkinham, J. O., III; Santos, W. L. Branched Peptides: Acridine and Boronic Acid Derivatives as Antimicrobial Agents. *ACS Med. Chem. Lett.* **2017**, *8*, 820−823.
(31) Graham, L. A.; Wilson, G. M.; West, T. K.; Day, C. S.; Kucera, G. L.; Bierbach, U. Unusual Reactivity of a Potent Platinum-Acridine Hybrid Antitumor Agent. *ACS Med. Chem. Lett.* **2011**, *2*, 687−691.
(32) Cerón-Carrasco, J. P.; Ruiz, J.; Vicente, C.; Haro, C.; Bautista, D.; Zuniga, J.; Requena, A. DFT Simulation of Structural and Optical Properties of 9-Aminoacridine Half-Sandwich Ru(II), Rh(III), and Ir(III) Antitumoral Complexes and Their Interaction with DNA. *J. Chem. Theory Comput.* **2017**, *13*, 3898−3910.
(33) Latterini, L.; Tarpani, L. Hierarchical Assembly of Nanostructures to Decouple Fluorescence and Photothermal Effect. *J. Phys. Chem. C* **2011**, *115*, 21098−21104.
(34) Mitra, P.; Chakraborty, P. K.; Saha, P.; Ray, P.; Basu, S. Antibacterial Efficacy of Acridine Derivatives Conjugated with Gold Nanoparticles. *Int. J. Pharm.* **2014**, *473*, 636−643.
(35) Sardar, S.; Chaudhuri, S.; Kar, P.; Sarkar, S.; Lemmensb, P.; Pal, S. K. Direct Observation of Key Photoinduced Dynamics in a Potential Nano-Delivery Vehicle of Cancer Drugs. *Phys. Chem. Chem. Phys.* **2015**, *17*, 166−177.
(36) Zhou, K.; Zhu, Y.; Yang, X.; Jiang, X.; Li, C. Preparation of Graphene-TiO2 Composites with Enhanced Photocatalytic Activity. *New J. Chem.* **2011**, *35*, 353−359.
(37) Xiong, Z.; Zhang, L. L.; Ma, J.; Zhao, X. S. Photocatalytic Degradation of Dyes Over Graphene-Gold Nanocomposites Under Visible Light Irradiation. *Chem. Commun.* **2010**, *46*, 6099−6101.
(38) Wu, T.; Liu, G.; Zhao, J.; Hidaka, H.; Serpone, N. Photoassisted Degradation of Dye Pollutants. V. Self-Photosensitized Oxidative Transformation of Rhodamine B under Visible Light Irradiation in Aqueous TiO_2 Dispersions. *J. Phys. Chem. B* **1998**, *102*, 5845−5851.
(39) Wu, J. M.; Kao, W. T. Heterojunction Nanowires of $Ag_xZn_{1-x}O$−ZnO Photocatalytic and Antibacterial Activities under Visible-Light and Dark Conditions. *J. Phys. Chem. C* **2015**, *119*, 1433−1441.
(40) Hoffmann, M. R.; Martin, S. T.; Choi, W.; Bahnemann, D. W. Environmental Applications of Semiconductor Photocatalysis. *Chem. Rev.* **1995**, *95*, 69−96.
(41) Woan, K.; Pyrgiotakis, G.; Sigmund, W. Photocatalytic Carbon-Nanotube-TiO_2 Composites. *Adv. Mater.* **2009**, *21*, 2233−2239.
(42) Luo, Q.-P.; Yu, X.-Y.; Lei, B.-X.; Chen, H.-Y.; Kuang, D.-B.; Su, C.-Y. Reduced Graphene Oxide-Hierarchical ZnO Hollow Sphere Composites with Enhanced Photocurrent and Photocatalytic Activity. *J. Phys. Chem. C* **2012**, *116*, 8111−8117.
(43) Hirakawa, T.; Kamat, P. V. Charge Separation and Catalytic Activity of Ag@TiO_2 Core-Shell Composite Clusters under UV-Irradiation. *J. Am. Chem. Soc.* **2005**, *127*, 3928−3934.
(44) Kannaiyan, D.; Kim, E.; Won, N.; Kim, K. W.; Jang, Y. H.; Cha, M.-A.; Ryu, D. Y.; Kim, S.; Kim, D. H. On the Synergistic Coupling Properties of Composite CdS/TiO_2 Nanoparticle Arrays Confined in Nanopatterned Hybrid Thin Films. *J. Mater. Chem.* **2010**, *20*, 677−682.
(45) Liu, S.; Yang, L.; Xu, S.; Luo, S.; Cai, Q. Photocatalytic Activities of C-N-Doped TiO_2 Nanotube Array/Carbon Nanorod Composite. *Electrochem. Commun.* **2009**, *11*, 1748−1751.
(46) Fukuzumi, S.; Kojima, T. Photofunctional Nanomaterials Composed of Multiporphyrins and Carbon-Based π-Electron Acceptors. *J. Mater. Chem.* **2008**, *18*, 1427−1439.

DOI: 10.1021/acsomega.8b00568
ACS Omega 2018, 3, 7962−7970

(47) Barman, M. K.; Mitra, P.; Bera, R.; Das, S.; Pramanik, A.; Patra, A. An Efficient Charge Separation and Photocurrent Generation in the Carbon dot-Zinc Oxide Nanoparticles Composite. *Nanoscale* **2017**, *9*, 6791−6799.
(48) Mitra, P.; Barman, M. K.; Basu, S.; Das, S.; Pramanik, A.; Patra, A. Interfacial Charge Transfer between Zinc Oxide Nanoparticles and Methyl Viologen: Influence of Size. *ChemistrySelect* **2017**, *2*, 9869−9877.
(49) Kar, P.; Sardar, S.; Alarousu, E.; Sun, J.; Seddigi, Z. S.; Ahmed, S. A.; Danish, E. Y.; Mohammed, O. F.; Pal, S. K. Impact of Metal Ions in Porphyrin-Based Applied Materials for Visible-Light Photocatalysis: Key Information from Ultrafast Electronic Spectroscopy. *Chem. - Eur. J.* **2014**, *20*, 10475−10483.
(50) Liu, D.; Lv, Y.; Zhang, M.; Liu, Y.; Zhu, Y.; Zong, R.; Zhu, Y. Defect-Related Photoluminescence and Photocatalytic Properties of Porous ZnO Nanosheets. *J. Mater. Chem. A* **2014**, *2*, 15377−15388.
(51) Tu, W.; Lei, J.; Wang, P.; Ju, H. Photoelectrochemistry of Free-Base-Porphyrin-Functionalized Zinc Oxide Nanoparticles and Their Applications in Biosensing. *Chem. - Eur. J.* **2011**, *17*, 9440−9447.
(52) Das, S.; Pramanik, S.; Chatterjee, S.; Das, P. P.; Devi, P. S.; Suresh Kumar, G. Selective Binding of Genomic *Escherichia coli* DNA with ZnO Leads to White Light Emission: A New Aspect of Nano−Bio Interaction and Interface. *ACS Appl. Mater. Interfaces* **2017**, *9*, 644−657.
(53) Zhang, J.; Zhao, B.; Pan, Z.; Gu, M.; Punnoose, A. Synthesis of ZnO Nanoparticles with Controlled Shapes, Sizes, Aggregations, and Surface Complex Compounds for Tuning or Switching the Photoluminescence. *Cryst. Growth Des.* **2015**, *15*, 3144−3149.
(54) Zhang, Y.; Jia, H.; Wang, R.; Chen, C.; Luo, X.; Yu, D.; Lee, C. Low-Temperature Growth and Raman Scattering Study of Vertically Aligned ZnO Nanowires on Si Substrate. *Appl. Phys. Lett.* **2003**, *83*, 4631−4633.
(55) Schuldiner, S.; Rottenberg, H.; Avron, M. Determination of ΔpH in Chloroplasts. 2. Fluorescent Amines as a Probe for the Determination of ΔpH in Chloroplasts. *Eur. J. Biochem.* **1972**, *25*, 64−70.
(56) Murza, A.; Sánchez-Cortés, S.; García-Ramos, J. V.; Guisan, J. M.; Alfonso, C.; Rivas, G. Interaction of the Antitumor Drug 9-Aminoacridine with Guanidinobenzoatase Studied by Spectroscopic Methods: A Possible Tumor Marker Probe Based on the Fluorescence Exciplex Emission. *Biochemistry* **2000**, *39*, 10557−10565.
(57) Vietmeyer, F.; Seger, B.; Kamat, P. V. Anchoring ZnO Particles on Functionalized Single Wall Carbon Nanotubes. Excited State Interactions and Charge Collection. *Adv. Mater.* **2007**, *19*, 2935−2940.
(58) Marczak, R.; Werner, F.; Gnichwitz, J.-F.; Hirsch, A.; Guldi, D. M.; Peukert, W. Communication via Electron and Energy Transfer between Zinc Oxide Nanoparticles and Organic adsorbates. *J. Phys. Chem. C* **2009**, *113*, 4669−4678.
(59) Pant, D. D.; Joshi, G. C.; Tripathi, H. B. Photophysics of 9-aminoacridinium Hydrochloride. *Pramana J. Phys.* **1986**, *27*, 161−170.
(60) Kathiravan, A.; Kumar, P. S.; Renganathan, R.; Anandan, S. Photoinduced Electron Transfer Reactions between meso-tetrakis(4-sulfonatophenyl)porphyrin and Colloidal Metal-Semiconductor Nanoparticles. *Colloids Surf. A* **2009**, *333*, 175−181.
(61) Sirelkhatim, A.; Mahmud, S.; Seeni, A.; Kaus, N. H. M.; Ann, L. C.; Bakhori, S. K. M.; Hasan, H.; Mohamad, D. Review on Zinc Oxide Nanoparticles: Antibacterial Activity and Toxicity Mechanism. *Nano-Micro Lett.* **2015**, *7*, 219−242.
(62) Brayner, R.; Ferrari-Iliou, R.; Brivois, N.; Djediat, S.; Benedetti, M. F.; Fiévet, F. Toxicological Impact studies Based on *Escherichia coli* Bacteria in Ultrafine ZnO Nanoparticles Colloidal Medium. *Nano Lett.* **2006**, *6*, 866−870.
(63) Zhang, H.; Lv, X.; Li, Y.; Wang, Y.; Li, J. P25−Graphene Composite as a High Performance Photocatalyst. *ACS Nano* **2010**, *4*, 380−386.
(64) Huang, Z.; Zheng, X.; Yan, D.; Yin, G.; Liao, X.; Kang, Y.; Yao, Y.; Huang, D.; Hao, B. Toxicological Effect of ZnO Nanoparticles Based on Bacteria. *Langmuir* **2008**, *24*, 4140−4144.
(65) Xia, T.; Kovochich, M.; Liong, M.; Madler, L.; Gilbert, B.; Shi, H.; Yeh, J. I.; Zink, J. I.; Nel, A. E. Comparision of the Mechanism of Toxicity of Zinc Oxide and Cerium Oxide Nanoparticles Based on Dissolution and Oxidative Stress Properties. *ACS Nano* **2008**, *2*, 2121−2134.
(66) Beane, G. A.; Morfa, A. J.; Funston, A. M.; Mulvaney, P. Defect-Mediated Energy Transfer between ZnO Nanocrystals and a Conjugated Dye. *J. Phys. Chem. C* **2012**, *116*, 3305−3310.
(67) Lakowicz, J. R. *Principles of Fluorescence Spectroscopy*; Plenum Press: New York, 2006.
(68) Chatterjee, A. K.; Sarkar, R. K.; Chattopadhyay, A. P.; Aich, P.; Chakraborty, R.; Basu, T. A Simple Robust Method for Synthesis of Metallic Copper Nanoparticles of High Antibacterial Potency against *E. coli*. *Nanotechnology* **2012**, *23*, No. 085103.
(69) Dutta, D.; Mukherjee, R.; Patra, M.; Banik, M.; Dasgupta, R.; Mukherjee, M.; Basu, T. Green Synthesized Cerium Oxide Nanoparticle: A Prospective Drug against Oxidative Harm. *Colloids Surf., B* **2016**, *147*, 45−53.
(70) Chatterjee, A. K.; Chakraborty, R.; Basu, T. Mechanism of Antibacterial Activity of Copper Nanoparticles. *Nanotechnology* **2014**, *25*, No. 135101.

DOI: 10.1021/acsomega.8b00568
ACS Omega 2018, 3, 7962−7970